Polymer solar cells based on poly(3-hexylthiophene) and fullerene: Pyrene acceptor systems

Alessandra Cominetti [a], Andrea Pellegrino [a], Luca Longo [a], Riccardo Po [a, *], Alessandra Tacca [a], Chiara Carbonera [a], Mario Salvalaggio [a], Michele Baldrighi [b, 1], Stefano Valdo Meille [b]

[a] *Research Center for Renewable Energies and Environment, Istituto Donegani, Eni S.p.A, Via Fauser 4, IT-28100 Novara, Italy*
[b] *Dipartimento di Chimica, Materiali e Ingegneria Chimica "G. Natta", Politecnico di Milano, via Mancinelli 7, IT-20131 Milano, Italy*

Received 12 May 2014
Received in revised form
30 January 2015
Accepted 27 March 2015
Available online 4 April 2015

1. Introduction

The literature on novel materials for polymer solar cells [1–3] deals mainly with the development of the donor components of the active layer [4–9], while much fewer papers are devoted to novel acceptors [10,11]. [6,6]-phenyl-C61-butyric acid methyl ester

* Corresponding author.
E-*mail address:* riccardo.po@eni.com (R. Po).
[1] Present address: Istituto Italiano di Tecnologia (IIT), via Morego 30, IT-16163 Genova, Italy.

(PCBM) is the oldest [12], the most used [13] and, to date, still one of the most effective acceptors for bulk heterojunction polymer solar cells. The popularity of PCBM, aside from its unique electronic properties, is mainly due to its good solubility in many organic solvents and easy processability of its blends. The methyl phenylbutyrate substituent imparts to PCBM – and to its C70 homologue (PC71BM) – proper miscibility with poly(3-hexylthiophene) (P3HT), as well as with other donor polymers, able to form the peculiar nanostructured percolating morphology required by the photoactive film. Alternative acceptors to PCBM and PC71BM exist, but are scarce. The indene-C60 bis adduct (ICBA) [14], indene-C60 mono adduct (ICMA) [15] and indene-C70 bis adduct [16,17] are very effective, also in tandem cells. Bis-PCBM [18] and endohedral fullerenes [19] showed some promises, but their high cost does not justify a possible use in large-area devices; other non-fullerene acceptors, e.g. peryleneimides [20] or vinazenes [21], did not achieve high performances to date.

On the other hand, unfunctionalized C60 and C70, which would be advantageous for their availability and relatively low cost, have been seldom used in bulk heterojunction solar cells, because of their low solubility [22–24] that causes aggregation and poor film morphology. Rait et al. reported power conversion efficiencies up to 2.1% for P3HT:C60 solar cells, by using trichlorobenzene as a solvent [25], but according to other authors [26] – and to our experience -the devices are scarcely reproducible. Motaung et al. reported P3HT:C60 solar cells with 0.029% efficiency [27]; prolonged annealing leads to larger C60 domains and lower efficiency. By using 1,2,4-trimethylbenzene solvent, Tada et al. obtained effi-ciencies of 0.87% and 1.47% for P3HT:C60 [27] and P3HT:C70 [28] solar cells, respectively. Better performances have been reported by Tang et al., who attained a good morphology control in P3HT:C70 blends by using a heptane/*o*-dichlorobenzene mixture as solvent and achieved a 2.24% efficiency [29], and by Chan et al. [30], who reported a P3HT:C60 device with 2.56% efficiency by using an alkyl thiophene/fullerene-substituted thiophene block copolymer as interfacial agent. In the latter paper, however, the preparations of the comonomer and the polymer are quite laborious. Finally, Lu et al. [31] engineered the morphology of C60, by creating a nanorod network in the P3HT matrix by CS_2 vapor treatment, and were able to increase the efficiency of the devices from 0.40% to 2.50%.

Here, we report a new and simple approach for P3HT:C60 and P3HT:C70 bulk heterojunction solar cells fabrication, by exploiting π-π interactions between fullerenes and pyrene to promote fullerene dispersion in the active blend.

2. Experimental part

2.1. Materials

P3HT (OS2100, Plextronics Inc.), C60 (Sigma–Aldrich), C70 (Sigma–Aldrich), 1-pyrenebutyric acid (Sigma Aldrich), n-butanol (Sigma Aldrich) were purchased in high purity grade and used as received.

2.2. Synthesis of butyl 1-pyrenebutyrate (PyBB)

To a 100 mL two-necked round bottom flask equipped with a magnetic stirrer, 879 mg of 1-pyrenebutyric acid, 50 mL of n-butanol and 1 mL of concentrated sulphuric acid were added, forming a suspension which became a solution upon heating to reflux temperature. After 3 h the solution was cooled to room temperature, and 200 mL of brine and 200 mL of ethyl acetate were added. The aqueous fraction was removed and the organic fraction was extracted three times (250 mL) with distilled water. The organic fraction was dried over anhydrous sodium sulphate, filtered, and the solvent was distilled under reduced pressure. 1.03 g (yield 84%) of a pale yellow oil were obtained, which became a white solid after 24 h of storage at +4 °C in a refrigerator. T_m = 37.4 °C (DSC). ^{1}H-NMR (CD_2Cl_2): 8.31 ppm (1H, H1′, d, $J_{1',2'} = 9.3$ Hz), 8.17 ppm (1H, H7′, d, $J_{7',8'} = 7.9$ Hz), 8.16 ppm (1H, H9′, d, $J_{9',8'} = 7.9$ Hz), 8.12 ppm (1H, H2′, d, $J_{2',1'} = 9.3$ Hz), 8.11 ppm (1H, H5′, d, $J_{5',6'} = 7.6$ Hz), 8.03 ppm (2H, H3′ e H4′, s br.), 7.99 ppm (1H, H8′, t, $J_{8',7,9'} = 7.6$ Hz), 7.87 ppm (1H, H6′, d, $J_{6',5'} = 7.7$ Hz), 4.11 ppm (2H, H1, t, $J_{1,2} = 6.7$ Hz), 3.40 ppm (2H, H5, t, $J_{5,6} = 7.7$ Hz), 2.46 ppm (2H, H7, t, $J_{7,6} = 7.3$ Hz), 2.20 ppm (2H, H2, m), 1.62 ppm (2H, H6, m), 1.39 ppm (2H, H3, m), 0.94 ppm (3H, H4, t, $J_{4,3} = 7.4$ ppm). The full spectrum is reported in Supporting Information (Figures S1 and S2).

2.3. Electrochemical analysis

The cyclovoltammetric (CV) characterizations were carried out with an Autolab PGSTAT 12 potentiostat, run by a PC with GPES software. The working cell included a Glassy Carbon (GC) disk embedded in Teflon® (Amel, surface 0.071 cm^2) as the working electrode, a Platinum counter electrode (Metrohm), and an aqueous saturated calomel electrode (SCE, Amel) as the reference electrode. Dissolved sample analysis: a solution of the sample ($\approx 2 \cdot 10^{-4}$ M) in 0.1 M tetrabutylammonium tetrafluoroborate TBATFB (Fluka, electrochemical grade) acetonitrile:*o*-dichlorobenzene 1:4, was purged with argon and analysed in the electrochemical cell. Film analysis: the sample was dissolved in chlorobenzene ($\approx$1 mg/ml) and drop coated from a capillary on the GC electrode. The electrolytic solution was acetonitrile (Carlo Erba, HPLC grade) with 0.1 M tetrabutylammonium tetrafluoroborate TBATFB (Fluka, electrochemical grade). The solution was degassed by argon purging. The scan rate was 200 mV s^{-1}. According to IUPAC recommendations, data have been referred to the Fc^+/Fc redox couple (ferricinium/ferrocene) [32]. E_{HOMO} and E_{LUMO} values were extrapolated from the onset peaks potential, according to the following semiempirical equation [33]:

$$E_{HOMO/LUMO} = \left[-e\left(E_{onset(vs\cdot SCE)} - E_{onset(Fc/Fc+vs\ SCE)}\right)\right] - 5.1eV.$$

2.4. Optical spectroscopy

UV–Vis absorption spectra of thin films spin–coated onto quartz substrates were acquired in transmission mode with a double beam double monochromator Perkin Elmer λ 950 spectrophotometer in the range 200–850 nm, with a bandwidth of 1 nm and stepwise of 1 nm.

2.5. Fabrication of photovoltaic devices

Standard solar cells were fabricated by first spin-coating 30 nm of PEDOT:PSS (Clevios P AI 4083, Heraeus GmbH) as buffer layer, filtered through a 0.45 μm filter, on top of ITO-coated glass substrates (15 Ω/sq, Kintec Co., Hong Kong) at 3000 rpm for 90 s and annealed at 120 °C for 10 min. The active layer (100 nm) was spin-coated at 600 rpm for 90 s on top of PEDOT:PSS from solution in chlorobenzene heated at 35 °C. The concentration of P3HT (Plexcore OS 2100, Plextronics Inc., Pittsburgh) was 10 mg/mL. The blend component ratios are given in Table 2. The devices were completed by the cathode deposition consisting either of 100 nm of aluminium or 15 nm of calcium and 100 nm of aluminium in a thermal evap-orator in a 10^{-6} Torr vacuum. C70 based solar cells were post-annealed on a hot plate at 150 °C for 30 min under nitrogen at-mosphere. Each substrate contained 3 cells, each with a nominal active area of 25 mm^2. The effective active area of each cell was measured with an optical microscope.

Inverted solar cells were fabricated by first spin-coating 30 nm of sol–gel ZnO precursor [34] on top of ITO-coated glass substrates at 600 rpm for 150 s and annealed at 140° C for 1 h. The active layer (100 nm) was spin-coated at 600 rpm for 90 s on top of ZnO from solution in chlorobenzene heated at 35 °C. The concentration of P3HT was 10 mg/mL. The blend component ratios are given in Table 2. 120 nm of PEDOT:PSS (Clevios CPP 105 D, Heraeus GmbH) buffer layer anode was spin-coated at 2000 rpm for 90 s and annealed at 120° C for 10 min. The devices were completed by the anode deposition consisting of 100 nm of silver in a thermal evaporator in a 10^{-6} Torr vacuum. Each substrate contained 3 cells, each with a nominal active area of 25 mm^2.

2.6. Testing of photovoltaic devices

Film thicknesses were measured on a Veeco Dektak 150 profilometer. Current-voltage characteristics were measured in glove-box by using a Keithley 2602 A sourcemeter. The light intensity of AM 1.5G sunlight from an Abet 2000 solar simulator was calibrated by a KG-5 filtered Si photodiode. Inverted solar cells were illumi-nated trough a 4 × 4mm^2 shadow mask. External quantum effi-ciencies (EQEs) were characterized using a Schreder GmbH (Kirchbichl, AT) system equipped with a Bentham TMc 300 and a certified mc-Si diode. Monochromatic light was generated from a dual light source (a Xe 150 W lamp and a QH 100 W lamp). The spot diameter was 1 mm.

2.7. Optical microscopy

The active blend films were examined by standard optical microscopy (Nikon Eclipse LV150). All images were taken in air and at room temperature. In order to obtain the absorption coefficients, average film thicknesses were measured by a Dektak 150 Surface Profiler (Veeco Metrology).

2.8. Modelling of PyBB-C60 complexes

All models of the molecules and of the complexes were obtained by Density Functional Theory (DFT) [35–38]. This approach, coupled with the choice of a Hybrid B3LYP exchange + correlation correction [39–41] was due to the electronic detail needed. Theoretical exploitation of π-π interactions between fullerenes and pyrene moieties to promote fullerene dispersion in the active blend, required the introduction of dispersion corrected DFT. The Grimme DFT-D3 method [42] was the natural choice due to its recognized ability to efficiently correct the well known underestimation of π-π interactions by standard Hybrid DFT.

2.9. Solid state synthesis and characterization of the PyBB-C70 complex

Solid-state synthesis of the supramolecular PyBB-C70 complex was performed by thermal treatment of PyBB and C70 in 1:1 mol:mol mixture. 30 mg of C70-fullerene (0.0357 mmol) were mixed with 12.36 mg (0.0357 mmol) of PyBB in a glass vial and heated at 150 °C in an N_2 purged oven for 120 min, periodically mixing the material. DSC measurements were performed using a Perkin Elmer DSC 8500 calorimeter calibrated with an indium standard and standard Al pans. Measurements were performed in N_2 atmosphere with a 10 °C/min scan rate. X-Ray powders patterns were acquired on a Bruker D2 diffractometer using Cu *Kα* radiation (λ = 1.54184 Å), 0.01°/step. Acquisition times varied depending on the characteristics of each sample in order to achieve good quality spectra. FTIR spectra were acquired on a Varian 660 FTIR spectrometer equipped with an Attenuated Total Reflectance (ATR) accessory.

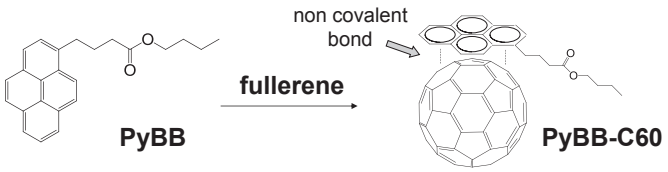

Fig. 1. Structure of butyl 1-pyrenebutyrate (PyBB) and formation of PyBB-C60 complex.

3. Results & discussion

Pyrene derivatives are well known to form non-covalent interactions with carbon nanotubes [43–45] and are used to favour the nanotubes dispersion in different solvents. Non-covalent functionalization of graphene [46,47] or fullerenes [48,49] with pyrene derivatives has seldom been addressed in the literature, but nevertheless demonstrated in some cases [46] to be an effective technique to prepare stable dispersions of otherwise very low soluble materials. Thus, with this idea in mind, a pyrene derivative with an alkyl ester chain has been synthesized starting from the commercially available 1-pyrenebutyric acid; the esterification with 1-butanol with H_2SO_4 catalyst proceeds smoothly, affording butyl 1-pyrenebutyrate (PyBB) in high yield and high purity. The PyBB structure and a plausible model for a complex with C60 fullerene (PyBB-C60) are shown in Fig. 1.

3.1. Molecular modeling

While the formation of complexes of pyrene and other polynuclear aromatics with C60 and C70 has been previously experimentally demonstrated by spectroscopic studies [50,51], a quantum mechanical study has been carried out to gain a more detailed understanding of such complexes. DFT modelling of several Polycyclic Aromatic Hydrocarbons (PAH), including PyBB, and of C60 and C70 fullerenes has been performed and the aggregation of the corresponding PAH-Cx (x = 60 or 70) complexes has been investigated.

The equilibrium intermolecular distance, estimated between the nearest couple of carbon atoms belonging to each molecule (see Table 1), is ~3 Å, considerably below the "non-interaction" distance, and decreases with the increase of the number of condensed aromatic rings. The enthalpy of the reaction PAH + Cx → PAH-Cx rises roughly by 3 kcal/mol for each aromatic ring of the PAH system, but levels off when the PAH comprises three aromatic rings, increasing only modestly with addition of further aromatic rings. This observation seems to correlate well with the calculated interaction geometry of the complexes: PAHs tend to arrange so that one of the carbon atoms shared by three of its condensed aromatic rings is the closest to the fullerene surface. In the case of fullerenes interacting with linear PAHs, two adjacent carbon atoms at the junction of condensed aromatic rings are the nearest atoms to the fullerene

Table 1
Closest optimized intermolecular distances and enthalpies of formation of PAH-Cx adducts.

Cx	PAH	Cx-PAH distance (Å)	ΔH (Kcal/mol)
C60	Benzene	3.64	−2.72
	Naphthalene	3.21	−6.51
	Anthracene	3.32	−8.05
	Phenanthrene	3.24	−8.72
	Pyrene	3.12	−9.14
	PyBB	3.08	−9.68
C70	Pyrene	3.15–3.30	−9.34
	PyBB	3.28	−11.60

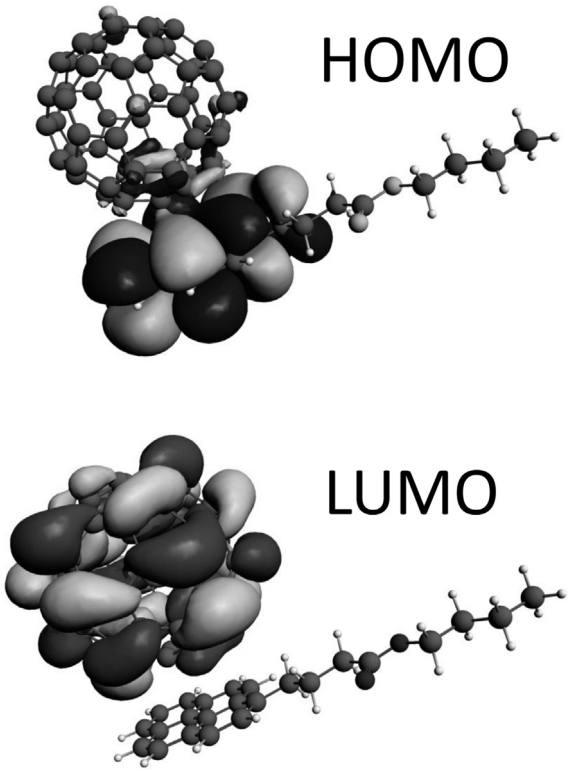

Fig. 2. Calculated HOMO (top) and LUMO (bottom) orbitals of PyBB-C60.

surface. On the other hand, all the Cx models investigated arrange themselves facing the PAH with a C6—C6 ring junction (Supporting Information, Figure S3). In C60 all the 30 C6—C6 ring junctions are equivalent, while in C70, there are four geometrically different C6—C6 ring junctions (Supporting Information, Figure S4): 10 around the "poles", 5 across the "equator", 10 across the "tropics" and 20 diagonally around the "tropics" (in Table 1, a range of distances is accordingly reported). Combined with C70, the pyrene system is preferentially located over one of the four regions described above. In the "equatorial" region two distinct relative minima were found, one with the pyrene mayor axis parallel to the C70 principal axis and one in which these two axes are perpendicular.

Analysis of the frontier orbitals of PyBB-Cx, shows that the Highest Occupied Molecular Orbital (HOMO) is localized on pyrene and on the fullerene portion closest to the pyrene molecule, while the corresponding Lowest Unoccupied Molecular Orbital (LUMO) is entirely located on the fullerene moiety (Fig. 2).

The calculated frontier orbitals energies of PyBB-C60 and PyBB-C70 are reported in Fig. 3 and compared to the experimental data obtained by cyclic voltammetry.

Considering the data in Fig. 3a, it is evident that while the HOMO energies of the complexes lie between those of their parent components, they are very close to the HOMO energy of PyBB (the difference is only 0.11 eV for both C60 and C70). This can be explained by the increase of the ionization potential of the pyrene component in the complex, due to electron depletion caused by the interaction with fullerene. Similarly, the LUMO energies of the complexes are intermediate between those of the precursors, but very close to the LUMO energy of the respective parent fullerene. The energy difference is 0.23 eV for C70 and 0.26 eV for C60. In this case, the pyrene molecule pushes electron density toward the fullerene, thus decreasing its electron affinity.

3.2. Solid-state characterization of the PyBB-C70 complex

In order to identify well defined experimental models of the PyBB-fullerene complexes, to be compared with theoretical results, various attempts to obtain cocrystals of PyBB with C60 and C70 fullerenes were performed. No strategy leading to crystallization of good quality single crystals from solution was successful, probably due to the very different solubility of fullerenes and the pyrene derivative in available organic solvents. DSC experiments were hence performed mixing the solid fullerenes with PyBB in 1:1 ratio inside the pans, and analysing the thermal behaviour of the mixture during the heating ramp. While for the PyBB-C60 mixture it was not possible to evidence any clear thermal event apart from the PyBB melting (37 °C), in the PyBB:C70 thermogram a second endothermic event at 166 °C is clearly visible, which is likely to correspond to the melting of a supramolecular complex formed during the PyBB melting (Fig. 4a). These results however do not preclude the possibility of significant favourable interactions between PyBB and C60 both in solution and in bulk. The presently

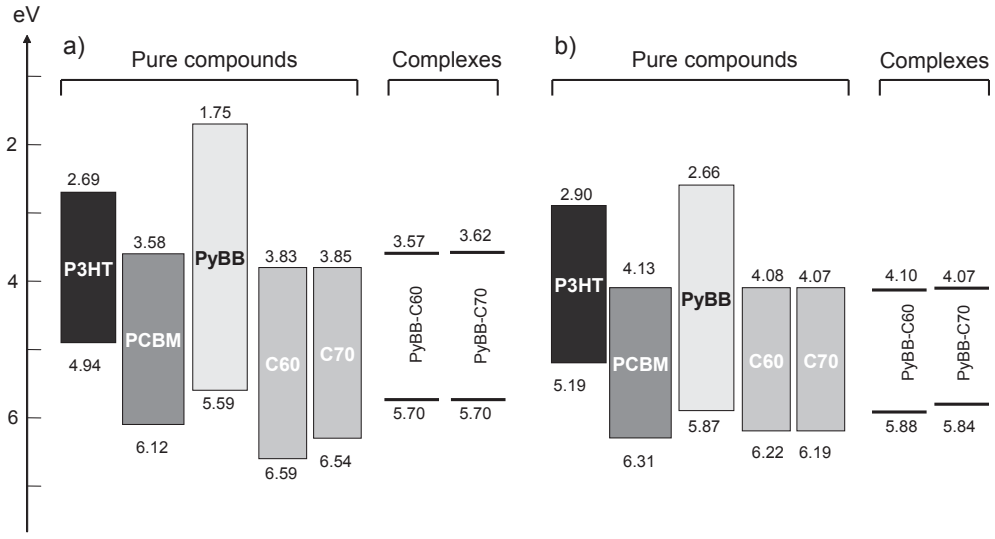

Fig. 3. Theoretical (a) and experimental (b) energy levels diagram.

available experimental evidence on the other hand clearly suggests that thermal annealing strategies can be used to generate crystalline solid supramolecular complexes between C70 and PyBB. It is hence likely that the behaviour of the electron acceptor component in devices containing both PyBB and C70 will be more complex than in the case where the active layer contains P3HT:PyBB-C60.

Larger quantities of PyBB-C70 than those used for DSC scans were prepared by thermal annealing of 1:1 mol:mol mixtures of the two starting components, The black solid thus obtained was ana-lysed by XRPD and (ATR)-FTIR spectroscopy. XRPD analysis confirmed that indeed a new crystalline phase had formed, as evidenced by the presence of a number of diffraction peaks which are not present in either of the starting materials (Fig. 4). A residual crystalline C70 phase component is however also present in all the prepared samples. Further addition of PyBB to the mixture and subsequent repetition of the thermal annealing procedure was so far unsuccessful in removing all the crystalline C70 traces: hence the formation of the crystalline PyBB-C70 supramolecular complex is not quantitative and so far we were unable to solve its crystal structure producing detailed molecular models.

(ATR)-FTIR analysis shows essentially all the bands due to both C70 and PyBB in PyBB-C70 resulting from the thermal annealing procedure, with some relatively small differences in the position of several bands (see Supporting Information, Figure S5). This behaviour appears to be consistent with the formation of a supramolecular complex between the two species.

The results discussed in this section confirm the quantum mechanical simulations results, indicating that PyBB is able to non-covalently interact in well defined patterns, at least with C70, in the case of which a crystalline complex is obtained. The fact that crystalline complexes were not obtained with C60 also agrees with a somewhat reduced effectiveness of interactions resulting from simulations. Furthermore, the success of the thermal procedure to obtain the crystalline PyBB-C70 suggests that the complex could form also in the annealing step of the organic solar cell, likely with implications on the cell's efficiency.

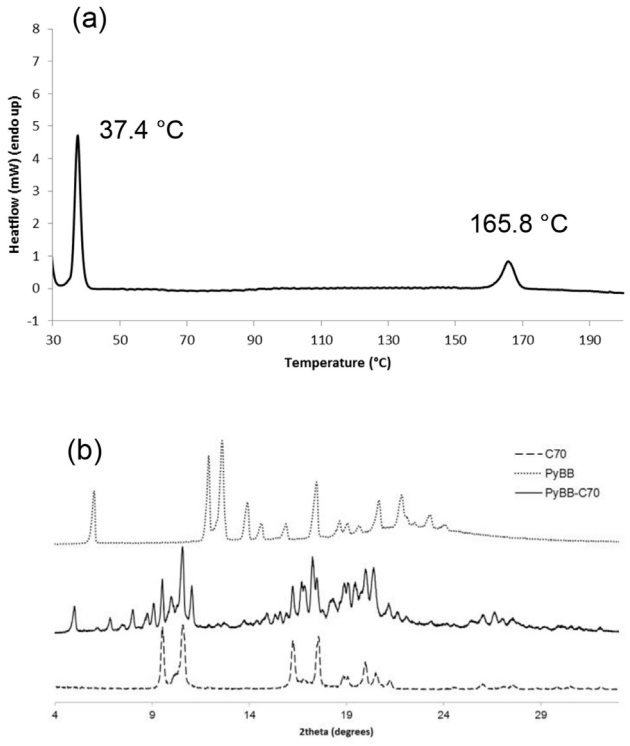

Fig. 4. a) DSC thermogram of PyBB-C70 complex and b) XRD diffractogram of C70 (dashed line), PyBB (dotted line) and PyBB-C70 (continuous line).

3.3. *Electrochemical properties*

Additional insight into the PyBB-C60 complex formation is provided by electrochemical measurements performed on the single components and on the mixtures of PyBB with the two fullerenes. The cyclovoltammetric (CV) analysis was carried out both on dissolved samples and on films drop cast on the working electrode. However, PyBB was characterized only in solution, considering its enhanced solubility in the electrolyte.

The HOMO and LUMO energy levels were extrapolated from the onset of the first oxidation and reduction peak potential and the values obtained for dissolved samples (in acetonitrile-dichlorobenzene 1:4) are reported in the experimental diagram shown in Fig. 3b. The energy levels of the mixture are almost superimposable with the corresponding ones of the single molecules (i.e. E_{HOMO} of PyBB and E_{LUMO} of fullerene). One possibility is in fact that the complex is dissolved in the electrolyte and/or is unable to react on the electrode surface. On the other hand, the values measured experimentally for the complexes correspond reasonably well to those calculated by modelling procedures, especially considering that complex formation may be not quantitative.

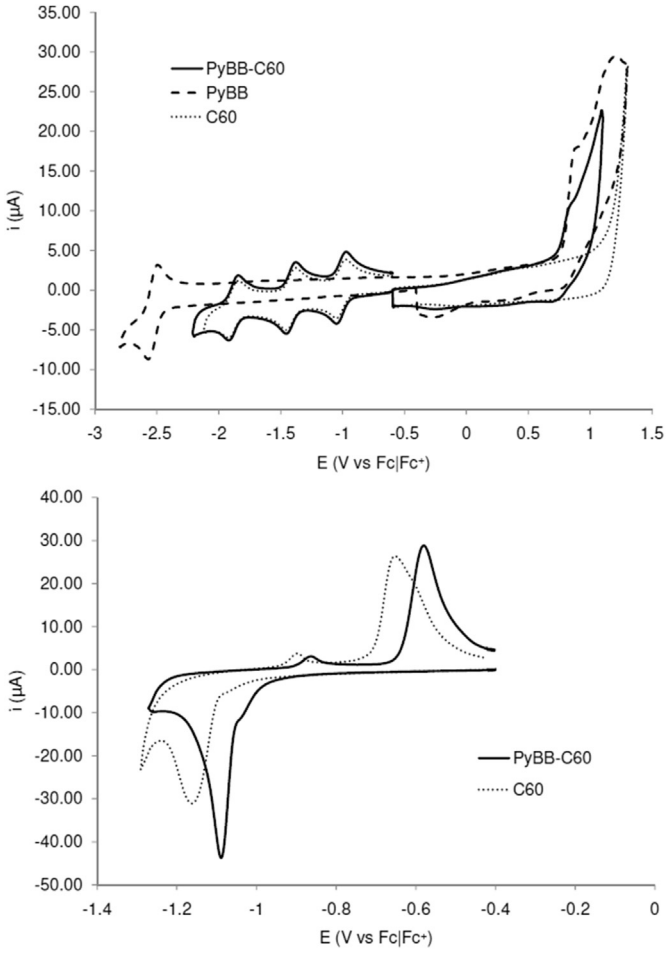

Fig. 5. Cyclic voltammograms of (top) PyBB-C60 (continuous line), PyBB (dashed line) and C60 (dotted line) dissolved in acetonitrile-dichlorobenzene 1:4 0.1 M TBATFB electrolyte; (bottom) PyBB-C60 (straight line) and C60 (dotted line) film drop-casted on the glassy carbon working electrode in acetonitrile 0.1 M TBATFB electrolyte (cathodic peaks).

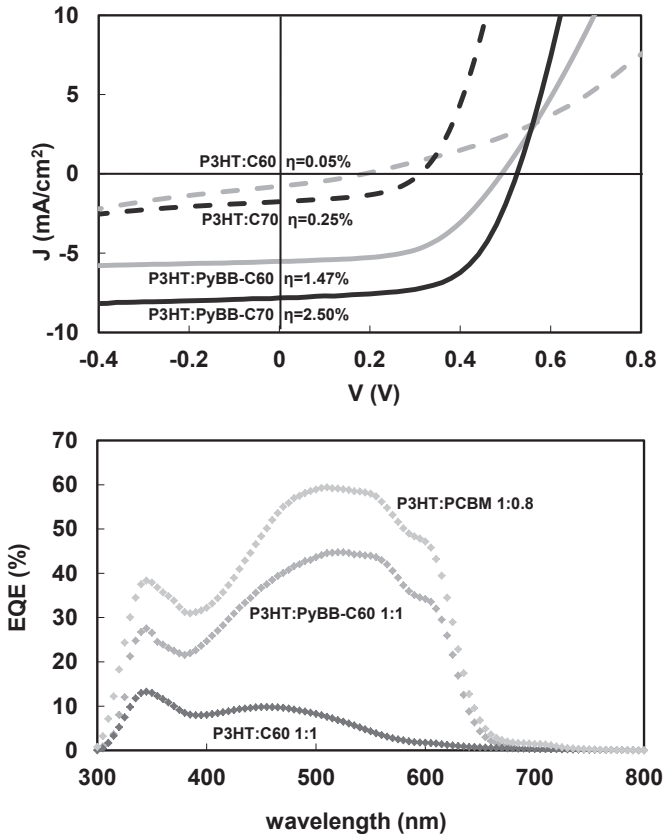

Fig. 6. Top: current–voltage curves of P3HT:C60, P3HT:C70, P3HT:PyBB-C60 and P3HT:PyBB-C70 solar cells with aluminium cathode; bottom: external quantum efficiency curves of solar cells with Ca/Al cathode (D:A ratios in w/w).

The cyclic voltammograms of PyBB-C60 are reported in Fig. 5a: it is evident that the curve of PyBB-C60 is composed by the oxidative signal of PyBB and the cathodic peaks of C60.

CV analysis performed on the film was corrupted by PyBB dissolution during the measurements. Notwithstanding, it seems that the reduction peak E_{max} of PyBB-C60 appears at a more positive potential than $E_{max,\ red}$ of neat C60 (Fig. 5b), while the onset potentials are very similar. According to the literature [52], the *maximum criterion* corresponds to the energy related to observation of maximum intensity of current. However, it is difficult to attribute this difference to the complex formation rather than to a stabilization of the film in the electrolyte, also considering that the large splitting between the reduction and reoxidation waves suggests reorganization of the film [53].

Moreover, in the PyBB-C70 case of study, E_{onset} and E_{max} are coincident both in film and in dissolved samples CV. All these occurrences make it unfeasible to demonstrate unequivocally the formation of the PyBB:Cx complexes through cyclovoltammetric measurements, while on the other hand not excluding this possibility.

3.4. Photovoltaic properties

Photovoltaic properties of P3HT:PyBB-Cx were investigated both in conventional (with either Al or Ca/Al cathode) and inverted solar cells. Reference devices with P3HT:Cx active layers were also prepared. Chlorobenzene was chosen as the solvent for the active blend deposition. In this solvent the solubility of C60 is 7 mg/mL [19]. Fig. 6 shows the J–V curves of the polymer solar cells under AM1.5G illumination at 100 mW/cm^2. Table 2 summarizes the main characteristics of the solar cells.

In agreement with previous reports [27] P3HT:C60 conventional solar cells have low power conversion efficiencies typically below 0.2%, mainly due to low photocurrents and poor fill factors. Addition of PyBB to the P3HT:C60 blend leads to power conversion efficiencies increased by an order of magnitude (Table 2). The presence of the additive does not alter the active layer thickness, which is around 110 nm in all cases. The higher efficiencies (around 1.5%) are obtained for the blend with 1:1 PyBB:C60 mol:mol ratio and P3HT: PyBB-C60 1:1 weight ratio, without thermal annealing. The change of the cathode from aluminium to calcium/aluminium does not cause significant variations, apart from a better reproducibility in devices preparation and performances. By increasing the PyBB:C60 ratio to 2:1 at constant donor/acceptor ratio, the efficiencies decrease to 0.3–0.6% (depending on the electrode material), likely due to the low fullerene concentration in the active blend. The effect of PyBB on C60 aggregation is shown in Fig. 7. Fig. 7a, representing P3HT:C60 without PyBB, shows the presence of large amounts of fullerene aggregates, strongly reduced when PyBB is added to the blend (Fig. 7b). In order to evidence the better morphology obtained with the addition of PyBB, micrograph (c), corresponding to (b) with enhanced contrast, is reported. Comparing pictures (a) and (c) the reduced amount and size of microcrystals in presence of PyBB is clearly apparent.

It must be remarked that the images have been taken on films prepared in the same conditions of those used in the devices except for the absence of the cathode. However, because it is known that

Table 2
Photovoltaic properties of unannealed conventional (C) and inverted (I) P3HT:PyBB:Cx (x = 60.70) solar cells. The best values and, in parentheses, the average values of three devices are reported.

Acceptor	Architecture	Annealing	Cathode	PyBB:Cx (mol:mol)	P3HT:Cx (wt:wt)	P3HT:PyBB-Cx (wt:wt)	Voc (V)	Jsc (mA/cm^2)	FF	η (%)
C60	C	No	Al	0	1:1	–	0.19 (0.20)	0.78 (0.76)	0.31 (0.30)	0.05 (0.05)
PyBB-C60	C	No	Al	1:1	1:0.68	1:1	0.49 (0.49)	5.51 (5.38)	0.54 (0.54)	1.47 (1.44)
PyBB-C60	C	No	Al	2:1	1:0.51	1:1	0.51 (0.46)	4.57 (4.30)	0.24 (0.23)	0.56 (0.45)
C60	C	No	Ca/Al	0	1:1	–	0.48 (0.36)	1.22 (1.10)	0.34 (0.31)	0.20 (0.13)
PyBB-C60	C	No	Ca/Al	1:1	1:0.68	1:1	0.50 (0.51)	5.15 (4.84)	0.56 (0.54)	1.46 (1.34)
PyBB-C60	C	No	Ca/Al	2:1	1:0.51	1:1	0.51 (0.51)	4.12 (3.81)	0.17 (0.17)	0.36 (0.32)
C60	I	No	–	0	1:1	–	0.42 (0.42)	2.19 (1.96)	0.52 (0.50)	0.49 (0.43)
PyBB-C60	I	No	–	1:1	1:0.68	1:1	0.50 (0.51)	7.62 (6.88)	0.59 (0.59)	2.25 (2.07)
C70	C	No	Al	0	1:1	–	0.019 (0.009)	1.86 (1.38)	0.007 (0.003)	3×10^{-5} (2×10^{-5})
C70	C	150 °C, 30 min	Al	0	1:1	–	0.32 (0.32)	1.58 (1.51)	0.50 (0.48)	0.25 (0.24)
PyBB-C70	C	No	Al	1:1	1:1	1:1.41	0.48 (0.37)	6.70 (6.31)	0.49 (0.39)	1.57 (1.03)
PyBB-C70	C	150 °C, 30 min	Al	1:1	1:1	1:1.41	0.53 (0.53)	7.82 (7.60)	0.61 (0.58)	2.50 (2.33)
PyBB-C70	C	No	Al	1:1	1:0.71	1:1	0.48 (0.48)	6.19 (5.76)	0.45 (0.45)	1.34 (1.25)
PyBB-C70	C	150 °C, 30 min	Al	1:1	1:0.71	1:1	0.52 (0.52)	7.42 (7.39)	0.54 (0.51)	2.08 (1.97)

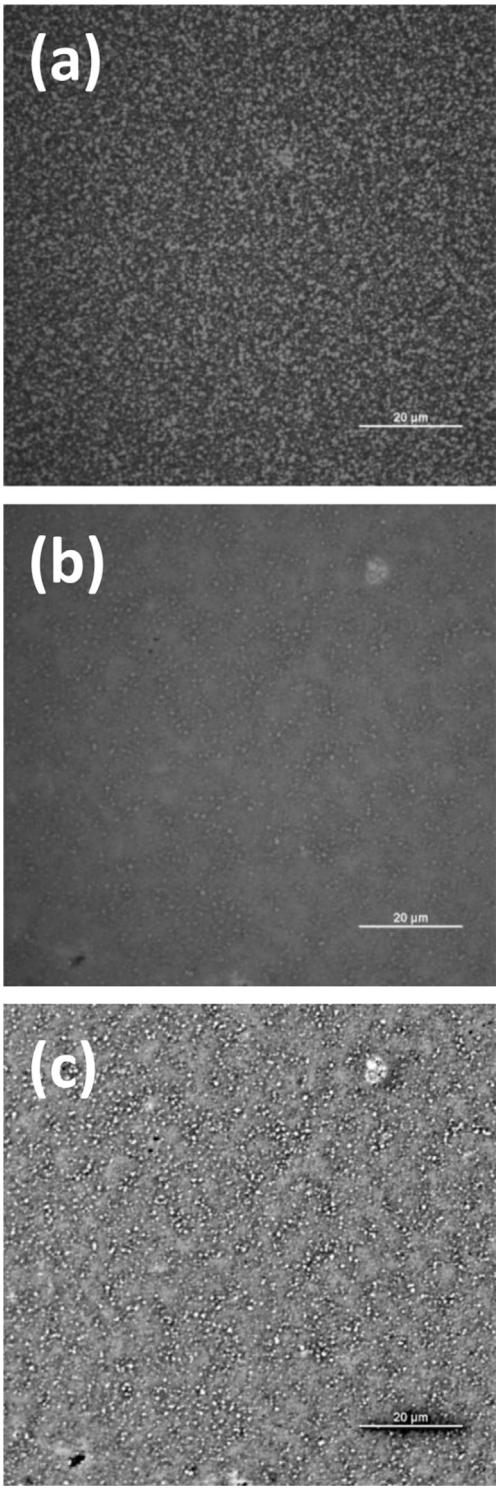

Fig. 7. Optical micrographs of (a) P3HT:C60 film; (b) P3HT:PyBB-C60 film . (c) same as picture (b), with enhanced contrast. Materials ratios are the same used in devices; the size of both crystals and of their aggregates would be substantially limited by the presence of the cathode. Marker length = 20 µm.

the cathode modifies the morphological evolution of the underneath film [54–56] it is likely that the observed morphologies are not entirely representative of the real situation in the cells, since fullerene crystals growth is reduced by the presence of the electrode. Quite probably, the presence of PyBB will additionally inhibit fullerene crystallization, even if to a degree difficult to quantify.

After thermal annealing at 150 °C for 30 min the efficiency drops dramatically (well below 0.1%). An almost complete disappearance of PyBB from the active layer thin films under these conditions was also revealed by UV–Vis analysis. The drop in efficiency is likely due to an unfavourable rearrangement of the donor and acceptor phases within the blend at the nanoscale, not discernible by optical microscopy, a situation plausibly induced by the depletion of PyBB from the active layer during the thermal treatment. Fig. 6 shows the EQE curves of P3HT:PyBB-C60, P3HT:C60 and, for comparison, of P3HT:PCBM conventional devices. P3HT:C60 external quantum efficiencies are very low, in agreement with the low efficiency value. EQE curve of P3HT: PyBB-C60 has the same shape of P3HT:PCBM, except perhaps a slightly increased response in the 420–490 nm range.

For the fabrication of large area modules, the choice of electrode materials is restricted by the necessity to achieve long-term stability in operating conditions and to use cheaper air-atmosphere processes. For these reasons the inverted geometry is, by far, preferable to the conventional architecture [34]. Thus ITO/ZnO/P3HT:PyBB-C60/MoO3/Ag solar cells have also been fabricated.

The efficiency of P3HT:C60 inverted device, prepared for comparison, is around 0.5% (Table 2). This relatively high value, compared to the conventional devices, could be tentatively attributed to a favourable vertical segregation of fullerene toward the bottom ITO/ZnO electrode during the spin coating deposition of the active layer, as suggested by the fairly high fill factor value. It is known indeed from the literature that the blend components are non-uniformly distributed in the vertical direction. For example, in P3HT:PCBM blends deposited on PEDOT:PSS or ZnO, P3HT - with lower surface energy compared to the fullerene derivative [57] - is preferentially attracted at the interface with air, while the high surface energy component (PCBM) tends to segregate at the hydrophilic bottom interface (i.e, PEDOT:PSS or ZnO) [54,58,59]. Thus, hypothesizing an acceptor-rich composition at the substrate interface (corresponding to the P3HT-rich free-air surface) the resulting vertical segregation of the donor/acceptor bi-continuous network should be favourable for inverted solar cells. In these devices the ITO/ZnO substrate acts as the collector of negative charge carriers. In inverted solar cells, the addition of PyBB leads to an efficiency of 2.25%, i.e. 4.6 times greater than that of P3HT:C60 reference device.

Turning now to C70, P3HT:C70 conventional solar cells (Table 2) have a negligible efficiency, that increases to 0.25% upon annealing; the fill factor is relatively high (0.50), i.e. significantly greater than that of P3HT:C60 conventional devices. Very likely, the poor performances are heavily affected by the presence of large fullerene crystals and aggregates (Fig. 8a), as in the case of C60-based devices.

Addition of PyBB to the P3HT:C70 blend dramatically improves the acceptor dispersion, as demonstrated by the optical micrographs (Fig. 8b). Upon thermal treatment at 150 °C for 30 min, the formation of sub-microaggregates is observed (Fig. 8c) but, as shown below, this phenomenon does not impair the devices performances. As commented with respect to Fig. 7 for C60, the presence of the cathode, actually limits crystal growth as compared to what is shown in Fig. 8, which is a qualitative evi-dence that PyBB additionally reduces crystal size. We should add that in the present case, along with C70 crystals, PyBB:C70 coc-rystals are likely to form as discussed above. Upon addition of PyBB, an improvement of photovoltaic parameters, especially Jsc, and efficiency (2.50%) is observed. The better efficiency of P3HT: PyBB-C70 conventional devices as compared to P3HT: PyBB-C60 cells, largely due to the higher J_{sc} (7.82 vs. 4.12 mA/cm^2), could be related to the higher molar extinction coefficient and the higher absorption of C70 in the 350–650 nm region, as compared

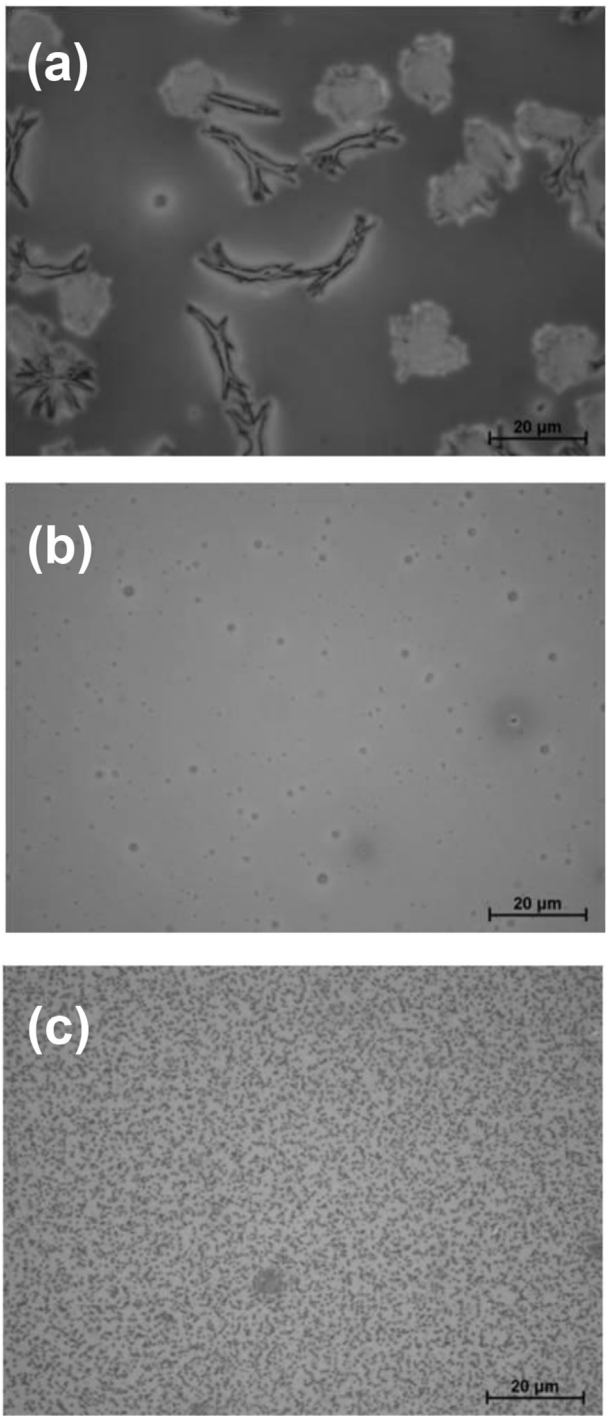

Fig. 8. Optical micrographs of (a) P3HT:C70 film; (b) P3HT:PyBB-C70 film; (c) P3HT:PyBB-C70 film annealed (150 °C, 30 min). Materials ratios are the same used in devices; the size of both the crystals and their aggregates would be substantially limited by the presence of the cathode. Marker length = 20 μm.

to C60 [60,61] and/or to factors relating to the PyBB:C70 complex formation. In fact, on the basis of the Eg values calculated and/or obtained by CV, an absorption around 650–700 nm is expected for PyBB-C70 adducts, even if it has never been clearly evidenced. Accordingly, the absorption coefficient of a P3HT: PyBB-C70 film was found to be significantly increased, compared to the one peculiar to P3HT: PyBB-C60 prepared with the same composition (Fig. 9): the higher absorbance of the P3HT: PyBB-C70 film in the

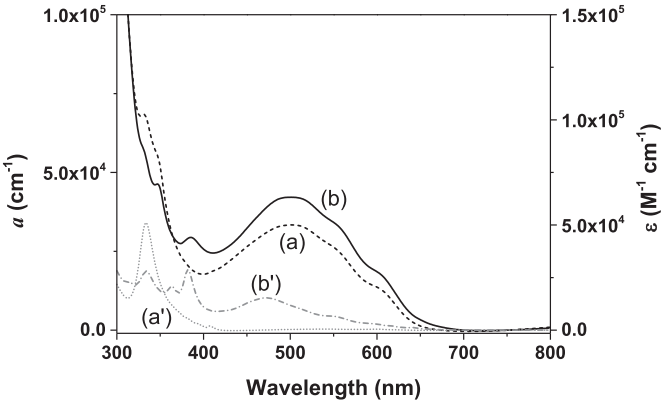

Fig. 9. Absorption coefficients $a(\lambda)$ of (a) P3HT:PyBB-C60 and (b) P3HT:PyBB-C70 films (100 nm thick), prepared with the same molar ratios and spin coated onto quartz substrates, together with the molar absorption coefficients $\varepsilon(\lambda)$ of (a') C60 and (b') C70 in chlorobenzene solutions.

visible region is clearly related to the higher molar absorption coefficient $\varepsilon(\lambda)$ in chlorobenzene solution of C70 in comparison to C60.

4. Conclusions

In conclusion, polymer solar cells based on P3HT and unfunctionalized fullerene (either C60 or C70) active blends can be fabricated by using a pyrene derivative to prevent the aggregation of fullerene and improve the active layer morphology. In the case of C70, the formation of PyBB:C70 cocrystals is also likely to play a role. Maximum power conversion efficiencies of 1.54% and 2.50% have been obtained by using, respectively, C60 or C70 as acceptor.

The use of cheap unfunctionalized fullerenes instead of more expensive functional compounds (PCBM, PC71BM, ICBA, etc.) paves the way to cost-effective devices and might increase the possibility to effectively bring the OPV technology to the industrial scale [34,62]. The formation of fullerene cocrystals may provide an alternative strategy to the chemical substitution approaches to modulate morphology, interfacial properties and - to some degree - also electronic properties of active layers components.

The demonstration of the effectiveness of the approach reported in this paper to P3HT:fullerene systems is, however, only a first step: work is in progress with other highly efficient low-bandgap donor polymers to assess the general validity and wide applicability of this promising method. In parallel, other additives alternative to pyrenebutiric butyl ester with extended π-conjugation will be screened.

Acknowledgement

The authors thank Silvia Spera (Eni) for NMR analysis.

Appendix A. Supplementary data

Supplementary data related to this article can be found on line.

References

[1] G. Li, R. Zhu, Y. Yang, Polymer solar cells, Nat. Phot. 6 (2012) 153–161.
[2] R. Po, M. Maggini, N. Camaioni, Polymer solar cells: recent approaches and achievements, J. Phys. Chem. C 114 (2010) 695–706.
[3] Y. Li, Molecular design of photovoltaic materials for polymer solar cells: toward suitable electronic energy levels and broad absorption, Acc. Chem. Res. 45 (2012) 723–733.

[4] R. Kroon, M. Lenes, J.C. Hummelen, P.W.M. Blom, B. De Boer, Small bandgap polymers for organic solar cells (polymer material development in the last 5 Years), Polym. Rev. 48 (2008) 531–582.

[5] J. Chen, Y. Cao, Development of novel conjugated donor polymers for high-efficiency bulk-heterojunction photovoltaic devices, Acc. Chem. Res. 42 (2009) 1709–1718.

[6] Y.J. Cheng, S.H. Yang, C.S. Hsu, Synthesis of conjugated polymers for organic solar cell applications, Chem. Rev. 109 (2009) 5868–5923.

[7] C.L. Chochos, S.A. Choulis, How the structural deviations on the backbone of conjugated polymers influence their optoelectronic properties and photovoltaic performance, Prog. Polym. Sci. 36 (2011) 1326–1414.

[8] P.L.T. Boudreault, A. Najari, M. Leclerc, Processable low-bandgap polymers for photovoltaic applications, Chem. Mater. 23 (2011) 456–469.

[9] L. Bian, E. Zhu, J. Tang, W. Tang, F. Zhang, Recent progress in the design of narrow bandgap conjugated polymers for high-efficiency organic solar cells, Prog. Polym. Sci. 37 (2012) 1292–1331.

[10] J.L. Delgado, P.A. Bouit, S. Filippone, M.A. Herranz, N. Martin, Organic photovoltaics: a chemical approach, Chem. Commun. 46 (2010) 4853–4865.

[11] P. Sonar, J.P. Fong Lin, K.L. Chan, Organic non-fullerene acceptors for organic photovoltaics, Energy Environ. Sci. 4 (2011) 1558–1574.

[12] J.C. Hummelen, B.W. Knight, F. Lepeq, F. Wudl, J. Yao, C.L. Wilkins, Preparation and characterization of fulleroid and methanofullerene derivatives, J. Org. Chem. 60 (1995) 532–538.

[13] M.T. Dang, L. Hirsch, G. Wantz, P3HT: PCBM, best seller in polymer photovoltaic research, Adv. Mater. 23 (2011) 3597–3602.

[14] Y. He, H.Y. Chen, J. Hou, Y. Li, Indene–C60 bisadduct: a new acceptor for high-performance polymer solar cells, J. Am. Chem. Soc. 132 (2010) 1377–1382.

[15] Y. Liu, J. Zhao, Z. Li, C. Mu, W. Ma, H. Hu, K. Jiang, H. Lin, H. Ade, H. Yan, Aggregation and morphology control enables multiple cases of high-efficiency polymer solar cells, Nat. Commun. 5 (2014) 5293.

[16] Y. He, G. Zhao, B. Peng, Y. Li, High-yield synthesis and electrochemical and photovoltaic properties of indene-C70 bisadduct, Adv. Funct. Mater. 20 (2010) 3383–3389.

[17] X. Guo, C. Cui, M. Zhang, L. Huo, Y. Huang, J. Hou, Y. Li, High efficiency polymer solar cells based on poly(3-hexylthiophene)/indene-C70 bisadduct with solvent additive, Energy Environ. Sci. 5 (2012) 7943–7949.

[18] M.A. Faist, P.E. Keivanidis, S. Foster, P.H. Wobkenberg, T.D. Anthopoulos, D.D.C. Bradley, J.R. Durrant, J. Nelson, Effect of multiple adduct fullerenes on charge generation and transport in photovoltaic blends with poly(3-hexylthiophene-2,5-diyl), J. Polym. Sci. B, Polym. Phys. 49 (2011) 45–51.

[19] R.B. Ross, C.M. Cardona, D.M. Guldi, S.G. Sankaranarayanan, M. Reese, N. Kopidakis, J. Peet, B. Walker, G.C. Bazan, E. Van Keuren, B.C. Holloway, M. Drees, Endohedral fullerenes for organic photovoltaic devices, Nat. Mater. 8 (2009) 208–212.

[20] V. Kamm, G. Battagliarin, I.A. Howard, W. Pisula, A. Mavrinskiy, C. Li, K. Müllen, F. Laquai, Polythiophene: perylene diimide solar cells – the impact of alkyl-substitution on the photovoltaic performance, Adv. Energy Mater. 1 (2011) 297–302.

[21] C.H. Woo, T.W. Holcombe, D.A. Unruh, A. Sellinger, J.M.J. Fréchet, Phenyl vs alkyl polythiophene: a solar cell comparison using a vinazene derivative as acceptor, Chem. Mater. 22 (2010) 1673–1679.

[22] Y. Marcus, A.L. Smith, M.V. Korobov, A.L. Mirakyan, N.V. Avramenko, E.B. Stukalin, Solubility of C60 fullerene, J. Phys. Chem. B 105 (2001) 2499–2506.

[23] R.S. Ruoff, D.S. Tse, R. Malhotra, D.L. Lorents, Solubility of fullerene (C60) in a variety of solvents, J. Phys. Chem. 97 (1993) 3379–3383.

[24] G. Yu, J. Gao, J.C. Hummelen, F. Wudl, A.J. Heeger, Polymer photovoltaic cells: enhanced efficiencies via a network of internal donor-acceptor heterojunctions, Science 270 (1995) 1789–1791.

[25] S. Rait, S. Kashyap, P.K. Bhatnagar, P.C. Mathur, S.K. Sengupta, J. Kumar, Improving power conversion efficiency in polythiophene/fullerene-based bulk heterojunction solar cells, Sol. Energy Mater. Sol. Cells 91 (2007) 757–763.

[26] K. Tada, M. Onoda, Poor man's green bulk heterojunction photocells: a chlorine-free solvent for poly(3-hexylthiophene)/C60 composites, Sol. Energy Mater. Sol. Cells 100 (2012) 246–250.

[27] D.E. Motaung, G.F. Malgas, C.J. Arendse, S.E. Mavundla, C.J. Oliphant, D. Knoesen, Thermal-induced changes on the properties of spin-coated P3HT: C60 thin films for solar cell applications, Sol. Energy Mater. Sol. Cells 93 (2009) 1674–1680.

[28] K. Tada, Yet another poor man's green bulk heterojunction photocells: annealing effect and film composition dependence of photovoltaic devices using poly(3-hexylthiophene):C70 composites prepared with chlorine-free solvent, Sol. Energy Mater. Sol. Cells 108 (2013) 82–86.

[29] H. Tang, G. Lu, X. Yang, The role of morphology control in determining the performance of P3HT/C-70 bulk heterojunction polymer solar cells, IEEE J. Sel. Top. Quantum. Elect. 16 (2010) 1725–1731.

[30] S.H. Chan, C.S. Lai, H.L. Chen, C. Ting, C.P. Chen, Highly efficient P3HT: C60 solar cell free of annealing process, Macromolecules 44 (2011) 8886–8891.

[31] G. Lu, L. Li, X. Yang, Creating a uniform distribution of fullerene C60 nanorods in a polymer matrix and its photovoltaic applications, Small 4 (2008) 601–606.

[32] G. Gritzner, J. Kuta, Recommendations on reporting electrode potentials in nonaqueous solvents, Pure Appl. Chem. 56 (1984) 461–466.

[33] S.W. Hwang, Y. Chen, Synthesis and electrochemical and optical properties of novel poly(aryl ether)s with isolated carbazole and p-quaterphenyl chromophores, Macromolecules 34 (2001) 2981–2986.

[34] R. Po, A. Bernardi, C. Calabrese, C. Carbonera, G. Corso, A. Pellegrino, From lab to fab: how must the polymer solar cells materials design change ? – an industrial perspective, Energy Environ. Sci. 7 (2014) 925–943.

[35] R.G. Parr, W. Yang, Density-functional Theory of Atoms and Molecules, Oxford University Press, New York and Oxford, 1989.

[36] C. Fonseca Guerra, O. Visser, J.G. Snijders, G. te Velde, E.J. Baerends, in: E. Clementi, C. Corongiu (Eds.), Methods and Techniques for Computational Chemistry, METECC-95, STEF, Cagliari, 1995, pp. 303–395.

[37] G. te Velde, F.M. Bickelhaupt, E.J. Baerends, S.J.A. van Gisbergen, C. Fonseca Guerra, J.G. Snijders, T. Ziegler, Chemistry with ADF, J. Comput. Chem. 22 (2001) 931–967.

[38] Baerends E.J, et al. ADF2012, SCM, Theoretical Chemistry, Vrije Universiteit, Amsterdam, The Netherlands, http://www.scm.com.

[39] E.J. Baerends, D.E. Ellis, P. Ros, Self-consistent molecular Hartree—Fock—Slater calculations I. The computational procedure, Chem. Phys. 2 (1973) 41–51.

[40] E.J. Baerends, D.E. Ellis, P. Ros, Self-consistent molecular Hartree—Fock—Slater calculations II. The effect of exchange scaling in some small molecules, Chem. Phys. 2 (1973) 52–59.

[41] G. te Velde, E.J. Baerends, Numerical integration for polyatomic systems, J. Comput. Chem. 99 (1992) 84–98.

[42] S. Grimme, J. Anthony, S. Ehrlich, H.J. Krieg, A consistent and accurate ab initio parametrization of density functional dispersion correction (DFT-D) for the 94 elements H-Pu, J. Chem. Phys. 132 (2010) 154104.

[43] G.J. Bahun, A. Adronov, Interactions of carbon nanotubes with pyrene-functionalized linear-dendritic hybrid polymers, J. Polym. Sci. A, Polym. Chem. 48 (2010) 1016–1028.

[44] P.D. Tran, A. Le Goff, J. Heidkamp, B. Jousselme, N. Guillet, S. Palacin, H. Dau, M. Fontecave, V. Artero, Noncovalent modification of carbon nanotubes with pyrene-functionalized nickel complexes: carbon monoxide tolerant catalysts for hydrogen evolution and uptake, Angew. Chem. Int. Ed. 50 (2011) 1371–1374.

[45] E. Schopf, R. Broyer, L. Tao, Y. Chen, H.D. Maynard, Directed carbon nanotube assembly using a pyrene-functionalized polymer, Chem. Commun. 24 (2009) 4818–4820.

[46] Y. Xu, H. Bai, G. Lu, C. Li, G. Shi, Flexible graphene films via the filtration of water-soluble noncovalent functionalized graphene sheets, J. Am. Chem. Soc. 130 (2008) 5856–5857.

[47] M. Zhang, R.R. Parajuli, D. Mastrogiovanni, B. Dai, P. Lo, W. Cheung, R. Brukh, P.L. Chiu, T. Zhou, Z. Liu, E. Garfunkel, H. He, Production of graphene sheets by direct dispersion with aromatic healing agents, Small 6 (2010) 1100–1107.

[48] Y. Matsuo, K. Morita, E. Nakamura, Penta(pyrenyl)[60]fullerenes: pyrene–pyrene and [60]fullerene–pyrene interactions in the crystal and in solution, Chem. Asian J. 3 (2008) 1350–1357.

[49] R.B. Martin, K. Fu, H. Li, D. Cole, Y.P. Sun, Interesting fluorescence properties of C60-centered dendritic adduct with twelve symmetrically attached pyrenes, Chem. Commun. 18 (2003) 2368–2369.

[50] S. Bhattacharya, S.K. Nayak, S. Chattopadhyay, M. Banerjee, A.K. Mukherjee, Study of ground state EDA complex formation between [70]fullerene and a series of polynuclear aromatic hydrocarbons, Spectrochim. Acta A Mol. Biomol. Spectrosc. 58 (2002) 289–298.

[51] K. Datta, M. Banerjee, B.K. Seal, A.K. Mukherjee, Ground state EDA complex formation between [60]fullerene and a series of polynuclear aromatic hydrocarbons, J. Chem. Soc. Perkin Trans. 2 (2000) 531–534.

[52] A. Tacca, R. Po, M. Caldararo, S. Chiaberge, L. Gila, L. Longo, P.R. Mussini, A. Pellegrino, N. Perin, M. Salvalaggio, A. Savoini, S. Spera, Ternary Thiophene-X-Thiophene semiconductor building blocks (X = Fluorene, Carbazole, Phenothiazine): modulating electronic properties and electropolymerization ability by tuning the X core, Electrochim. Acta 56 (2011) 6638–6653.

[53] C. Jehoulet, Y.S. Obeng, Y. Kim, F. Zhou, A.J. Bard, Electrochemistry and Langmuir trough studies of C60 and C70 films, J. Am. Chem. Soc. 114 (1992) 4237–4247.

[54] M. Campoy-Quiles, T. Ferenczi, T. Agostinelli, P.G. Etchegoin, Y. Kim, T.D. Anthopoulos, P.N. Stavrinou, D.D.C. Bradley, J. Nelson, Morphology evolution via self-organization and lateral and vertical diffusion in polymer: fullerene solar cell blends, Nat. Mater. 7 (2008) 158–164.

[55] D.S. Germack, C.K. Chan, B.H. Hamadani, L.J. Richter, D.A. Fischer, D.J. Gundlach, D.M. DeLongchamp, Substrate-dependent interface composition and charge transport in films for organic photovoltaics, Appl. Phys. Lett. 94 (2009) 233303.

[56] J.J. Richards, A.H. Rice, R.D. Nelson, F.S. Kim, S.A. Jenekhe, C.K. Luscombe, D.C. Pozzo, Modification of PCBM crystallization via incorporation of C60 in polymer/fullerene solar cells, Adv. Funct. Mater. 23 (2013) 514–522.

[57] J.Y. Oh, W.S. Jang, T.I. Lee, J.M. Myoung, H.K. Baik, Driving vertical phase separation in a bulk-heterojunction by inserting a poly (3-hexylthiophene) layer for highly efficient organic solar cells, Appl. Phys. Lett. 98 (2011) 023303.

[58] S.A. Mauger, L. Chang, S. Friedrich, C.W. Rochester, D.M. Huang, P. Wang, A.J. Moulé, Self-Assembly of selective interfaces in organic photovoltaics, Adv. Funct. Mater. 23 (2013) 1935–1946.

[59] Z. Xu, L.M. Chen, G. Yang, C.H. Huang, J. Hou, Y. Wu, G. Li, C.S. Hsu, Y. Yang, Vertical phase separation in poly(3-hexylthiophene): fullerene derivative blends and its advantage for inverted structure solar cells, Adv. Funct. Mater. 19 (2009) 1227–1234.

[60] M.E. El-Khouly, M.Y. Araki, M. Fujitsuka, O. Ito, Photoinduced electron transfer between metal octaethylporphyrins and fullerenes (C60/C70) studied by laser flash photolysis: electron-mediating and hole-shifting cycles, Phys. Chem. Chem. Phys. 4 (2002) 3322–3329.
[61] T. Kesti, N. Tkachenko, H. Yamada, H. Imahori, S. Fukuzumi, H. Lemmetyinen, C70 vs C60 in zinc porphyrin–fullerene dyads: prolonged charge separation and ultrafast energy transfer from the second excited singlet state of porphyrin, Photochem. Photobiol. Sci. 2 (2003) 251–258.
[62] G. Marzano, C.V. Ciasca, F. Babudri, G. Bianchi, A. Pellegrino, R. Po, G.M. Farinola, Organometallic approaches to conjugated polymers for plastic solar cells: from laboratory synthesis to industrial production, Eur. J. Org. Chem. 30 (2014) 6583–6614.